TELKOMNIKA, Vol. 13, No. 4, December 2015, pp. 1289~1297
ISSN: 1693-6930, accredited A by DIKTI, Decree No: 58/DIKTI/Kep/2013
DOI: 10.12928/TELKOMNIKA.v13i4.3103

An Automatic Calibration Method for Near-infrared Camera in Optical Surgical Navigation

Rong Qian Yang[1], Xuan Si[1], Qin Yong Lin[1], Ken Cai*[2]
[1]Department of Biomedical Engineering, South China University of Technology, Guangzhou, 510006, China
[2]School of Information Science and Technology, Zhongkai University of Agriculture and Engineering, Guangzhou, 510225, China
*Corresponding author, e-mail: icken@126.com

Abstract

Optical surgical navigation system (SNS) with near-infrared tracking system is becoming extensively used in clinics, and the accuracy of SNS is influenced by the calibration of near-infrared cameras (NIRCs). We propose an automatic calibration method for NIRCs. The method is based on a designed calibration board. In our experiments, corners are automatically extracted to obtain the parameters of NIRCs. This method has the advantages of saving time, efficiency in computation, high accuracy, and reliability. In our experiments, an NIRC can be calibrated in only 5 s. Meanwhile, the average relative errors of the focal length and principal point are 0.87% and 1.39%, respectively.

Keywords*: Camera calibration, Calibration board, Corner extraction, Near-infrared camera*

1. Introduction

Camera calibration is an important issue in binocular vision system. The purpose of camera calibration is to determine the mapping transformation between image and world coordinates of objects [1]. In surgical navigation system, the binocular vision system is composed of two near-infrared cameras (NIRCs) [2-5]. The precision of NIRC calibration determines the performance of the entire navigation system. As such, NIRCs must be calibrated accurately.

Camera calibration methods for visible cameras are generally divided into two categories, namely, traditional calibration method and self-calibration method [6]. The traditional calibration method based on a pattern has high precision and usually has two stages [7–11], namely, direct linear transformation and nonlinear optimization. The method proposed by Zhang is more flexible because it uses a planar pattern [12]. A limitation of the traditional method is that it needs a calibration pattern with a known structure. The self-calibration method has low precision, but it is extensively used because it directly extracts environmental information as calibration information [13].

The NIRC is composed of a visible camera and near-infrared filter, so the pattern used in the traditional calibration method cannot be sensed by NIRCs. Several studies have used the calibration result of a camera without filter as the calibration result of NIRCs. Other researchers used an external light source to ensure that the NIRCs sense the calibration board, such as a checkerboard. However, the traditional calibration method cannot meet the need for accuracy, and the self-calibration method is influenced by light from the surroundings. This study proposes a direct NIRC calibration method using an NIRC calibration board, which consists of 64 (8 × 8) near-infrared surface-mounted diodes (NIR-SMDs).

In our previous work [14], we designed a calibration board, which has 64 (8 × 8) NIR-SMDs on a breadboard. In the present study, the calibration board is improved. We design the calibration board by constructing a printed circuit board (PCB) using a 5 V direct current (DC) power adapter as the supply voltage, which ensures that the current flowing through the calibration board is more stable to achieve more accurate calibration results. If the exact geometric information of the board is unknown, the board cannot be used directly for calibrating NIRCs. We use a calibrated binocular vision system composed of two visible cameras to obtain the geometric information of the board. Our previous work can use the designed board and

Received September 16, 2015; Revised November 2, 2015; Accepted November 14, 2015

existing calibration method to calibrate the NIRCs. However, human–computer interaction is needed during the procedure. The operator has to select the corners in the calibration board image manually, which means that the entire process is tiresome and time consuming. Moreover, the method cannot implement automation for calibration.

This study mainly considers two aspects. First, we design a calibration board using PCB and obtain its structural information using the existing method for NIRCs. Second, we propose an automatic calibration method for NIRCs, in which the human–computer interaction is not required. Results show that the proposed method significantly reduces the calibration time.

2. Design of the Calibration Board for NIRCs and Extraction of Geometric Information

Given that NIRCs can sense near-infrared light only, the texture of the calibration board for visible camera cannot be sensed. Thus, designing a board that can meet the need of NIRC calibration is necessary.

In this study, we design a calibration board based on NIR-SMDs. The circuit of the calibration board is designed and constructed using a PCB. On this board, 64 NIR-SMDs are arranged in an array of (8 × 8) with a rectangular net shape. The size of each diode is 1.6 mm × 0.8 mm × 0.3 mm. The size of the light-emitting point is 0.3 mm × 0.3 mm, with a wavelength of 940 nm. A 5 V DC power adapter is used as supply voltage for the board to ensure that the current flowing through NIR-SMDs is stable. The luminance of the light-emitting points can be modified by adjusting the variable resistor on the board to achieve Gaussian distribution for the grayscale of light spots in the image sensed by NIRCs and extract the subpixel coordinates of the light-emitting points. The designed calibration board for NIRCs has the following advantages. First, compared with the common calibration board, near-infrared light from NIR-SMDs can be sensed by NIRCs. Second, the luminance of light-emitting points can be adjusted to meet the need of NIRC calibration. Third, 64 light-emitting points are sufficient to compute the parameters of NIRCs.

We should obtain accurate geometric information of the board to calibrate the NIRCs with the designed board. A binocular vision system composed of two visible cameras (MV-130UM) is designed to obtain this information. After calibrating the system according to Zhang's work, it can be used to obtain the calibration pattern for NIRCs. Several images in different positions are captured in a darkroom to avoid interference from environmental light when extracting the subpixel coordinates. The new calibration pattern can be obtained according to our previous work [15]. The 3D coordinates of each point on the pattern can also be acquired. The calibration pattern with known geometric information is then obtained and shown in Figure 2, which can be used to calibrate NIRCs directly.

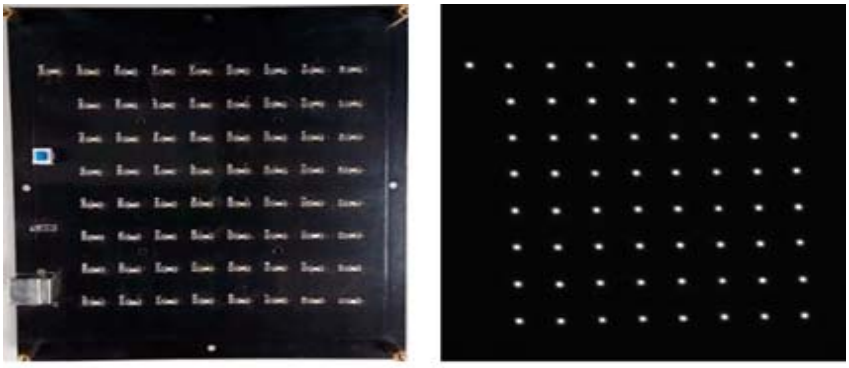

Figure 1. Designed calibration board (a) captured by the visible camera and (b) captured by the NIRC

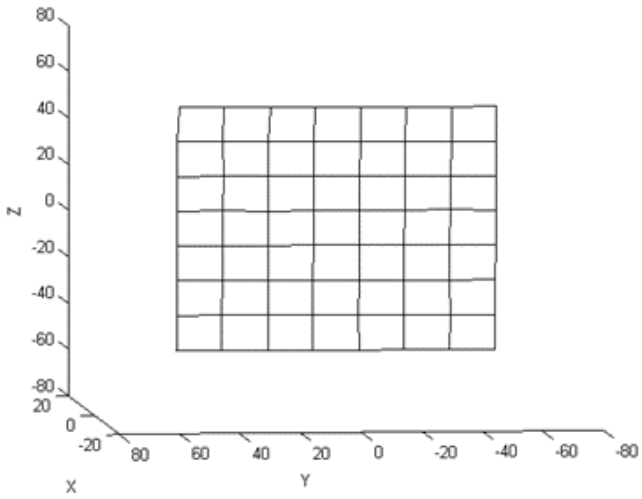

Figure 2. Calibration pattern

3. Automatic Calibration Method for NIRCs Based on a Pattern

The purpose of camera calibration is to compute the internal and external parameters of cameras. The automatic calibration method for NIRCs proposed in this study is based on and improves Zhang's two-stage camera calibration method [16]. First, classical pinhole imaging is adopted as the model of NIRCs. The distortion model is then introduced [17]. The parameters of NIRCs are calculated based on the distortion model.

Considering that our research is mainly used for binocular vision system in surgical navigation, only the radial and tangential distortions should be considered, as expressed in expression (1), in which $x^2 + y^2 = r^2$ and $k = [k_1, k_2, p_1, p_2, 0]^T$ is the lens distortion coefficient of NIRCs:

$$\begin{bmatrix} \delta_x \\ \delta_y \end{bmatrix} = \begin{bmatrix} x(1+k_1r^2+k_2r^4) \\ y(1+k_1r^2+k_2r^4) \end{bmatrix} + \begin{bmatrix} 2p_1xy + p_2(2x^2+r^2) \\ 2p_2xy + p_2(2y^2+r^2) \end{bmatrix}. \quad (1)$$

As shown in Figure 3, the process of NIRC calibration is mainly divided into three steps. First, the positions of the NIRCs relative to the calibration board are adjusted to keep the light-emitting points from spreading around the center of the image and capture a series of images of the calibration board in different positions. Second, the subpixel coordinates of feature points are computed using the method of gray-weighted average. The position and order of the four corners based on the triangular mesh method are also determined. The 2D information in each image of the calibration board is then acquired. Finally, the point-to-point correspondence between the subpixel coordinates of each light-emitting point and the 3D coordinates of each point on the calibration pattern must be established to obtain the parameters. The initial parameters are estimated using a linear estimation method, and the distortion model is introduced. The parameters are optimized using the method of nonlinear estimation. In this process, the innovative point is the automatic detection of the corners, which is the foundation of automatic calibration.

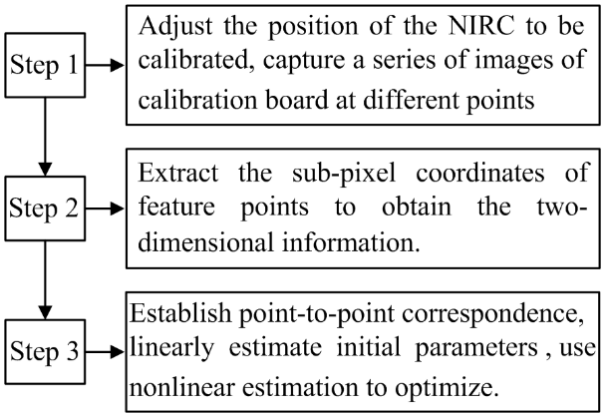

Figure 3. Process of NIRC calibration

In step 2, four initial values of light spots are obtained using automatic corner detection in each image. Corner detection is always a difficult problem in camera calibration [18]. Operators have to use the artificial or human–computer interaction by clicking the mouse to extract and obtain more precise information, which is tiresome and time consuming [19–21]. In this study, an automatic corner detection method based on the triangular mesh method is proposed using the NIRC calibration board designed previously.

A flag point is set at the beginning of the (8 × 8) NIR-SMD array in the designed calibration board. The flag point is near the point at the first row of the first column, as shown in Figure 1. The images captured by the NIRC are saved. The light-emitting points have a high contrast with the background. Thus, the images do not need filtering, which can improve the speed of searching feature points. We use the subpixel coordinates to characterize the light-emitting points in the images to improve precision. The method proposed in Ref. [16] is used to extract the subpixel coordinates of the feature points and obtain 2D information. The extraction result of the subpixel coordinates is shown in Figure 4(b).

After the subpixel coordinates of the feature points are obtained, the image is processed using the triangular mesh method. Using the subpixel points as the triangle vertices, the image is divided into a few triangle areas to determine the position and order of corners. An example of the results is shown in Figure 5(a).

The sum of the vertex angle of the triangles in every feature point is calculated. Assuming that the value of the sum is M, as shown in Figure 5(a), the value of M in the flag point is significantly less than 90°. After determining the position of the flag point, its triangular mesh is deleted, as shown in Figure 5(b). We then continue to calculate M. The value of M is close to 90° when the corners are selected as the vertex. The value of M is close to 180° or 360° when the other points are selected as the vertex. The positions of the flag point and four corners can be determined through the value of M. The first and third corners are determined using the distance between the corners and flag point. When calculating the distance between the flag point and each corner, the nearest is the first corner and the farthest is the third corner. The second and fourth corners are determined by calculating the angles. The flag point is denoted as P_f. The first and third corners are denoted as P_1 and P_3, respectively. The other two unsure corners are denoted as P_m and P_n. We set α as the angle between vector P_fP_1 and vector P_1P_m and β as the angle between vector P_fP_1 and vector P_1P_n. If angle α is less than angle β, then P_m is the second corner and P_n is the fourth corner. Otherwise, P_m is the fourth corner and P_n is the second corner. Based on the aforementioned process, the corners are automatically detected and their orders in each image are the same. Finally, the 2D information in each image of the calibration board is acquired.

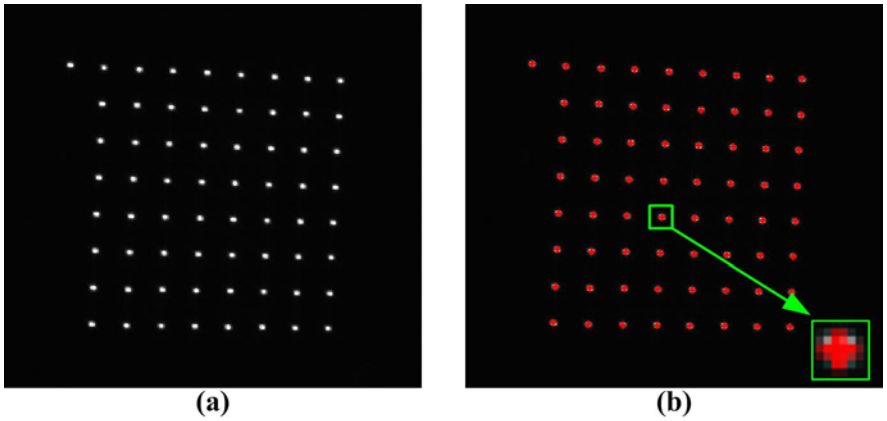

Figure 4. (a) Original image of the calibration board captured by NIRC and (b) subpixel extraction results, where "+" represents the subpixel coordinates

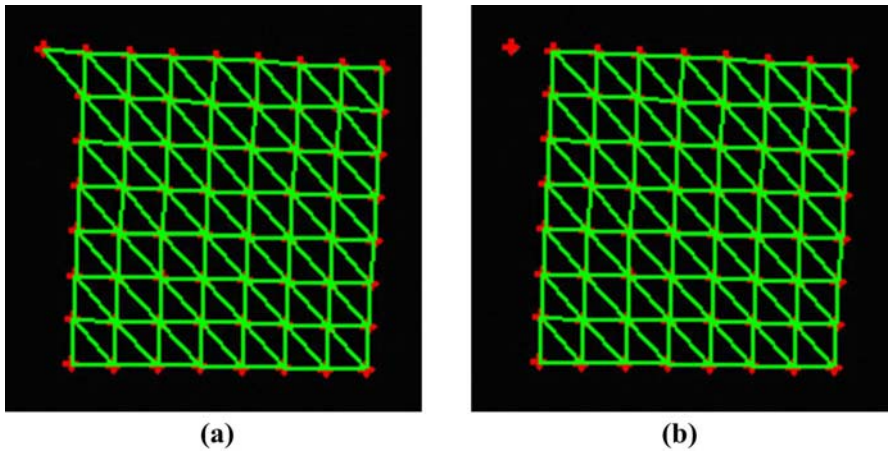

Figure 5. (a) Triangular mesh result of the subpixel points and (b) triangular mesh result of the subpixel points, except for the flag point

Assuming that P is a point in global space and $p(x_p, y_p)$ is its camera coordinate captured by the NIRCs, we derive expression (2), which can be expressed in matrix form in expression (3) as follows:

$$\begin{bmatrix} x_p \\ y_p \end{bmatrix} = \begin{bmatrix} f_x\left(\delta_x + \alpha\delta_y\right) + u_0 \\ f_y\delta_y + v_0 \end{bmatrix} \tag{2}$$

$$\begin{bmatrix} x_p \\ y_p \\ 1 \end{bmatrix} = \begin{bmatrix} f_x & \alpha f_x & u_0 \\ 0 & f_y & v_0 \\ 0 & 0 & 1 \end{bmatrix} \begin{bmatrix} \delta_x \\ \delta_y \\ 1 \end{bmatrix} \tag{3}$$

The matrix of the NIRC intrinsic parameters can be expressed as follows:

$$A = \begin{bmatrix} f_x & \alpha f_x & u_0 \\ 0 & f_y & v_0 \\ 0 & 0 & 1 \end{bmatrix} \tag{4}$$

In expression (4), f_x, f_y are the focal lengths of the camera, (u_0, v_0) are the coordinates of the main point of the camera, and α is the tilt factor of the two-image coordinate axis.

First, the NIRCs are considered an approximately ideal pinhole model when estimating the initial parameters of NIRCs, which means $k = 0$.

We set:

$$M = A\begin{bmatrix} R & T \end{bmatrix} = \begin{bmatrix} m_{11} & m_{12} & m_{13} & m_{14} \\ m_{21} & m_{22} & m_{23} & m_{24} \\ m_{31} & m_{32} & m_{33} & m_{34} \\ m_{41} & m_{42} & m_{43} & m_{44} \end{bmatrix} \tag{5}$$

For the ith feature point selected in the calibration process, with coordinates of (u_i, v_i, 1) in the image coordinate system and (X_{Wi}, Y_{Wi}, Z_{Wi}, 1) in the world coordinate system, we derive expression (6), which can be converted into the linear equations expressed in expression (7) as follows:

$$Z_{Ci}\begin{bmatrix} u_i \\ v_i \\ 1 \end{bmatrix} = \begin{bmatrix} m_{11} & m_{12} & m_{13} & m_{14} \\ m_{21} & m_{22} & m_{23} & m_{24} \\ m_{31} & m_{32} & m_{33} & m_{34} \\ m_{41} & m_{42} & m_{43} & m_{44} \end{bmatrix}\begin{bmatrix} X_{Wi} \\ Y_{Wi} \\ Z_{Wi} \\ 1 \end{bmatrix} \tag{6}$$

$$\begin{cases} m_{11}X_{Wi} + m_{12}Y_{Wi} + m_{13}Z_{Wi} + m_{14} - m_{31}u_iX_{Wi} - m_{32}u_iY_{Wi} - m_{33}u_iZ_{Wi} = m_{34}u_i \\ m_{21}X_{Wi} + m_{22}Y_{Wi} + m_{23}Z_{Wi} + m_{24} - m_{31}v_iX_{Wi} - m_{32}v_iY_{Wi} - m_{33}v_iZ_{Wi} = m_{34}v_i \end{cases} \tag{7}$$

For any feature point in the calibration process, we derive the two linear equations expressed in expression (7). Thus, for N feature points, $2N$ linear equations can be obtained. The matrix can be computed by solving the linear equations. For a total of 12 unknowns in M, the value of N must be greater than 6.

The result obtained using the aforementioned method is not highly accurate because it does not consider distortion. Distortion is introduced to enhance accuracy. Assuming that a total of N images are captured and for 64 feature points in every image, we can obtain $64N$ coordinates of pixels when the feature points are extracted. We set the real pixel coordinate of the ith feature point as $p_i(x_{pi}, y_{pi})$ and the ideal pixel coordinate obtained using the aforementioned method as $p_i'(u_i, v_i)$. Based on the nonlinear model with the influence of distortion, p_i, p_i' are fitted according to the objective function, as shown in expression (8):

$$\min E = \frac{1}{64 \times N}\sum_{i=1}^{64\times N}(u_i - x_{pi})^2 + (v_i - y_{pi})^2 \tag{8}$$

We set the value obtained using the aforementioned method as the optimized initial value of the nonlinear iterations. We then use iterative optimization by the least square method to derive the global optimum solution. Thus, the intrinsic parameters are obtained. The relative position relationship between the NIRCs and calibration board in every position, which are the extrinsic parameters, are simultaneously obtained.

4. Experimental Results

In this section, we concentrate on the comparison between the manual calibration method and automatic calibration method proposed in this study.

The NIRC captures 80 images of the calibration board, which are evenly divided into four groups. For each group, the results of the manual and automatic calibration methods are shown in Table 1. Notably, the results of the manual and automatic calibration methods are the same, thereby indicating that the automatic calibration method can reliably calibrate NIRCs.

The times consumed by the manual and automatic calibration methods in calibrating the four groups are shown in Table 2. The mean time consumed by the manual calibration method is 124 s, and the mean time consumed by the automatic calibration method is 5.57 s. This result shows that the proposed automatic calibration method significantly reduces the calibration time of the NIRCs.

As shown in Table 1, the mean relative errors of the focal lengths and principal points for the four groups are 0.84% and 1.46%, 0.76% and 0.88%, 1.03% and 1.74%, and 0.86% and 1.48%, respectively. The total mean relative errors of the focal lengths and principal points are 0.87% and 1.39%, respectively. Table 3 shows the mean relative errors of the focal lengths and principal points for the visible cameras used in Refs. [8], [22], and [23]. These results indicate that the proposed automatic calibration method is accurate and satisfactory.

For group 1, 20 images of the calibration board at different positions are captured by the NIRC. These images contain 1280 reprojection coordinates. Meanwhile, a total of 1280 residuals are acquired and shown in Figure 6. The reconstruction results of the 3D coordinates are shown in Figure 7. The residuals of the *X*-direction mainly concentrate in the interval of −0.15 pixels to 0.15 pixels, in which the number of feature points is 1270, accounting for 99.2% of the total. The residuals of the *Y*-direction mainly concentrate in the interval of −0.1 pixels to 0.1 pixels, in which the number of feature points is 1268, accounting for 99.1% of the total. The results of our previous work reported in Ref. [14] are −0.6 pixels to 0.6 pixels (95.7%) in the *X*-direction and −0.5 pixels to 0.5 pixels (92.2%) in the *Y*-direction. These results indicate that the new calibration board has higher precision, and it can describe the NIRC projection process correctly using the imaging geometry model established by the calibration results.

Table 1. Results of the manual and automatic calibration methods

	Group 1	**Group 2**	**Group 3**	**Group 4**
Manual (fc: mm)	[2115.84, 2115.20] ± [17.30, 18.19]	[2101.81, 2103.79] ± [15.83, 16.29]	[2046.79, 2043.75] ± [220.48, 21.65]	[2100.44, 2101.05] ± [018.27, 17.86]
Automatic (fc: mm)	[2115.84, 2115.20] ± [2115.8, 18.19]	[2101.81, 2103.79] ± [215.83, 16.29]	[2046.79, 2043.75] ± [220.48, 21.65]	[2100.44, 2101.05] ± [218.27, 17.86]
Manual (cc: pixels)	[631.42, 618.77] ± [311.53, 6.78]	[692.42, 609.50] ± [97.13, 4.65]	[645.41, 565.05] ± [414.53, 6.91]	[614.98, 571.18] ± [111.50,6.25]
Automatic (cc: pixel)	[631.42, 618.77] ± [311.53, 6.78]	[692.42, 609.50] ± [97.13, 4.65]	[645.41, 565.05] ± [414.53, 6.91]	[614.98, 571.18] ± [111.50,6.25]

Table 2. Time consumed by the manual and automatic calibration methods

	Group 1	Group 2	Group 3	Group 4
Manual	125 s	122 s	129 s	120 s
Automatic	5.28 s	5.34 s	5.87 s	5.78 s

Table 3. Mean relative errors

	Ref. [8]	Ref. [22]	Ref. [23]	This paper
Focal length	6.82%	0.57%	6.22%	0.87%
Principal point	4.44%	1.20%	0.56%	1.39%

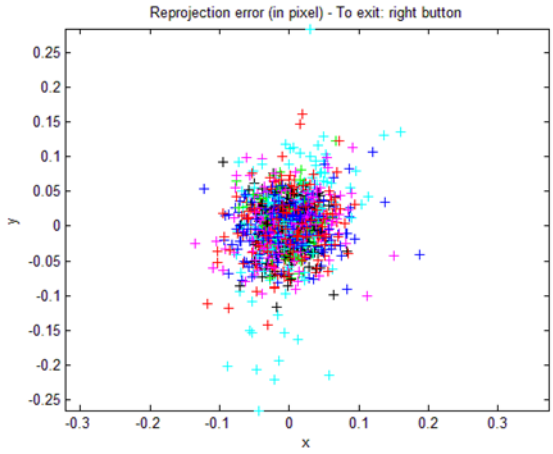

Figure 6. Reprojection error analysis

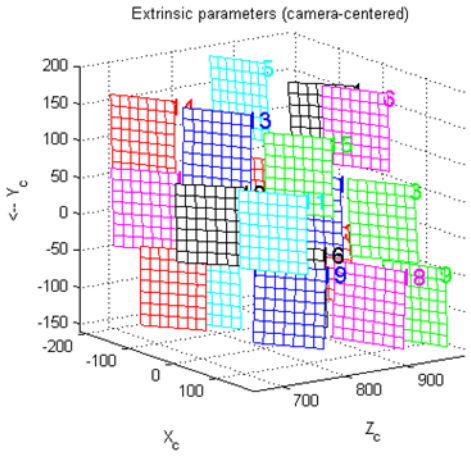

Figure 7. Reconstruction results of the 3D coordinates at different positions

5. Conclusions

This paper proposes an automatic calibration method to calibrate NIRCs. A calibration board with NIR-SMDs is designed because the common calibration board cannot be captured by NIRCs. Accurate geometric information is measured using a visible binocular vision system. The calibration pattern is obtained, which can be used to calibrate the NIRCs directly. The initial parameter values are obtained using direct linear transformation to calibrate the NIRCs. More accurate parameters are then achieved by the nonlinear optimization method. In the process of algorithm implementation, the 2D information of the image of the calibration board is automatically accessed.

The results of our experiments show that the average relative errors of the focal length and principal point of NIRC are 0.87% and 1.39%, respectively, which indicate that the proposed method has high accuracy. The time consumed by the automatic calibration process is 5.57 s, and the time consumed by the manual calibration method is 124 s. These findings indicate that the proposed method significantly reduces the calibration time.

In summary, the proposed NIRC automatic calibration method has the advantages of saving time, efficiency in computation, high accuracy, and reliability.

Acknowledgement

This research was funded by the Guangdong Natural Science Foundation under Grant No. S2013040014993, the State Scholarship Fund under Grant CSC NO. 201408440326, the Pearl River S&T Nova Program of Guangzhou under Grant No. 2014J2200049 and No. 201506010035, the Guangdong Provincial Science and Technology Program under Grant No. 2013B090600057 and No. 2014A020215006, the Fundamental Research Funds for the Central Universities under Grant No. 2014ZG003D.

References

[1] Sun JH, Chen X, Gong Z, Liu Z. and Zhao YT. "Accurate camera calibration with distortion models using sphere images". *Optics & Laser Technology*. 2015; 65: 83-87.
[2] Labudzki R, Legutko S, Raos P. The essence and applications of machine vision. *Tehnicki Vjesnik*. 2014; 21(4): 903-909.
[3] Kalomiros JA, Lygouras J. Hardware principles for the design of a stereo-matching state machine based on dynamic programming. *Journal of Engineering Science and Technology Review*. 2008; 1(1): 19-24.
[4] Cai K, Yang R, Ning H, Ou S, Zeng Z. An automatic algorithm for distinguishing optical navigation markers used during surgery. *DYNA*. 2015; 90(2): 203-209.
[5] Zhang XD, Hou ML, Hu YY, Zhang XQ, Wu YH. Study on the 3D information reconstruction and management of cultural relics based on the articulated arm scanner. *Journal of Digital Information Management*. 2015; 13(1): 31-38.
[6] Li XC, Wang YH. Automatic Selection for Optimal Calibration Model of Camera. *TELKOMNIKA Indonesian Journal of Electrical Engineering.* 2014; 12(3):4648-4653.
[7] Samper D, Santolaria Jorge, Majarena AC, Aguilar JJ. Comprehensive simulation software for teaching camera calibration by a constructivist methodology. *Measurement: Journal of the International Measurement Confederation*. 2010; 43(5): 618-630.
[8] Wang RY, Guang J, Quan L, Wu CK. Camera calibration using identical objects. *Machine Vision and Applications*. 2012; 23(3): 579-587.
[9] Wan YW, Huang Y, Buckles B. Camera calibration and vehicle tracking: Highway traffic video analytics. *Transportation Research Part C: Emerging Technologies*. 2014; 44: 202-213.
[10] John K. A camera calibration method for a hammer throw analysis tool. *Procedia Engineering*. 2014; 72: 74-79.
[11] Gao JC, Liu MY. Camera SelfCalibration in the AUV Monocular Vision Navigation and Positioning. *TELKOMNIKA Indonesian Journal of Electrical Engineering*. 2013; 11(12): 7151-7158.
[12] Zhang ZY. A flexible new technique for camera calibration. *IEEE Transactions on Pattern Analysis and Machine Intelligence*. 2000; 22: 1330-1334
[13] Yang XF, Huang YM, Gao F. A simple camera calibration method based on sub-pixel corner extraction of the chessboard image. *Intelligence Computing and Intelligent System.* 2010; 29-31.
[14] Wen XY, Liu SJ, Yang RQ, Wang ZG. Pattern design and realization for calibration near infrared camera in surgical navigation. *Optoelectronics Letters*. 2012; 8(6): 409-413.
[15] Zheng BS, Ji JP, Yang RQ. Calibration study of high-precision near infrared camera. *Chinese Medical Equipment Journal*. 2011; 32(12): 15-17.
[16] Wang ZG. Study of technique for optical tracking surgical instrument in surgery navigation. *A Dissertation Submitted for the Degree of Master: South China University of Technology*. 2012.
[17] William TR, Megeath ST. Martin C. Absolute calibration of the infrared array camera on the spritzer space telescope. *Publications of the Astronomical Society of the Pacific*. 2005; 117(835): 978-990.
[18] Xia JX, Xiong JL, Xu XQ, Qin HY. A multiscale sub-pixel detector for corners in camera calibration targets. *2010 International Conference on Intelligent Computation Technology and Automation*. 2010; 196-199.
[19] Chen DZ, Zhang GJ. A new sub-pixel detector for X-corners in camera calibration targets. *The 13th International Conference in Central Europe on Computer Graphics, Visualization and Computer Vision 2005 in co-operation with EUROGRAPHICS*. 2005; 97-100.
[20] Li LL, Zhao WC, Wu F, Liu Y, Gu W. Experimental analysis and improvement on camera calibration pattern. *Optical Engineering*. 2014; 53 (1): 013104.1-7.
[21] Arturo E, Jose MA. Automatic chessboard detection for intrinsic and extrinsic camera parameter calibration. *Sensors*. 2010; 10: 2027-2044.
[22] Jamil D, Sebastien R, Peter S. Plane-based calibration for linear cameras. *International Journal of Computer Vision*. 2011; 91: 146-156.
[23] Luis P, Yalin B, Peter S. Calibration of central catadioptric cameras using a DLT-like approach. *International Journal of Computer Vision*. 2011; 93: 101-114.